Sirte University Scientific Journal Vol. 15, No. 2 (2025) 37-41

Sirte University Scientific Journal (SUSJ)

Journal home page: http://journal.su.edu.ly/index.php/SUSJ/index
DOI: 10.37375/susj.v15i2.3721

Reducing Oxidation through Multi-Technique Synthesis: Impact on Phase Purity of Fe-Sb Alloys via XRD and Microstructural Study

Tarek Mohamed Fayez[1], Wesam Ahmed Mohamed Zeyara[2], Ibrahim A. Saleh [3], Abdelkhader Ali Abobaker [4]

[1]*Department of Physics, Sebha University, Libya*
[2]*Department of Physics, Fezzan University, Libya*
[3]*Department of Physics, Benghazi University, Libya*
[4]*Department of Renewable Energy, Sebha University, Libya*

DOI: https://doi.org/10.37375/susj.v15i2.3721

ARTICLE INFO:

Received 25 July 2025.
Accepted 07 October 2025.
Available online 24 December 2025.

Keywords:

Fe-Sb alloys, Phase purity, Oxidation control, X-ray diffraction, Microstructural analysis

A B S T R A C T

In this study, Fe-Sb alloy samples were synthesized using various processing techniques with the aim of reducing oxidation and enhancing phase purity. While samples S1 and S2 were prepared in a tube furnace under nitrogen atmosphere, sample S3 was synthesized using a vacuum-assisted current-heating method. X-ray diffraction (XRD) analysis revealed a multiphase composition, with $FeSb_2$ emerging as the dominant phase in the S3 sample. Secondary phases such as elemental Sb, metallic Fe, and a trace amount of Sb_2O_3 were also identified. Scanning electron microscopy (SEM) and energy dispersive X-ray spectroscopy (EDX) confirmed the correlation between the synthesis environment, oxidation degree, and microstructural uniformity. The vacuum-based synthesis of sample S3 effectively minimized oxygen incorporation, resulting in improved phase formation and structural integrity. These findings suggest that controlled synthesis under vacuum conditions is essential for optimizing Fe-Sb alloy systems, particularly when targeting intermetallic phases like $FeSb_2$ with minimal oxide contamination.

1 Introduction

Iron antimonide compounds, especially $FeSb_2$, are gaining attention due to their exceptional thermoelectric properties and potential use in energy conversion devices [1,2,3]. $FeSb_2$, a narrow-gap semiconductor, is especially notable for its colossal Seebeck coefficient at low temperatures, a behavior linked to strong electron correlations [1]. Studies have shown that this material exhibits large anisotropy in magnetoresistance and a spin-state transition, reinforcing its classification as a Kondo insulator [4,5]. In some alloy compositions, such as $FeSb_2$, it is preferable to avoid the presence of oxygen or the formation of oxides because the desired phase does not contain oxygen at all. Its presence may lead to changes in the chemical and crystalline structure. The presence of oxygen can cause deterioration in mechanical properties and negatively affect electrical or thermal conductivity due to the formation of insulating oxides. It may also accelerate corrosion and distort the crystalline structure of the alloy, weakening overall performance and hindering precise applications that require specific and stable properties. So, it is important to find a way to minimize the contribution of oxygen during the interaction process.

The optimization of Fe-Sb-based materials often revolves around precise control of phase composition and synthesis parameters, as multiple structural and magnetic phases such as FeSb, $FeSb_2$, elemental Sb, and oxides like Sb_2O_3 can form during

***Corresponding author*: E-mail:** tar.ahmad@sebhau.edu.ly

processing [6,7]. Understanding the phase stability and the ternary phase diagram of Fe-Sb systems is therefore crucial for tailoring the desired phase assemblage [7]. Recent approaches have emphasized chemical and solvothermal synthesis techniques for nanostructured $FeSb_2$ to enhance thermoelectric performance [3,8], while others have highlighted the importance of spark plasma sintering and reactive sintering for dense, pure intermetallic phases for Fe-Si alloys [9]. Additionally, studies investigating the time-dependent resistivity behavior of Fe-Sb alloys have underscored the sensitivity of their electronic properties to microstructural and compositional variations [10]. The introduction of novel synthesis strategies, including vacuum-assisted processing and mechanical alloying, has further enabled the reduction of oxidation and enhancement of phase purity in binary compounds such as Fe-Mn alloy [11,12]. These advancements are particularly relevant in the context of emerging applications, ranging from thermoelectrics to environmental and biomedical fields [13,14].

In this work, we examine the impact of different synthesis techniques on the structure and composition of Fe-Sb alloys. Three samples were prepared using solid-state reactions: two under nitrogen atmosphere (S1 and S2), and one using vacuum-assisted current heating (S3). X-ray diffraction XRD (PANalytical X'Pert PRO MRD PW3040), scanning electron microscopy SEM (JOEL JSM-6460LV) with an ET detector, and energy-dispersive X-ray spectroscopy EDX (Oxford instruments Analytical Ltd.) were used to evaluate phase composition, microstructure, and oxidation. The study aims to determine how synthesis atmosphere and heating method influence the formation of the desired $FeSb_2$ phase and the reduction of oxidation-related byproducts such as Sb_2O_3.

2 Experimental Setup

The FeSb alloy samples S1, S2, and S3 were synthesized by heating mixtures of high-purity starting materials (i.e., Fe and Sb powders), weighed in stoichiometric molar ratios. The starting materials were thoroughly mixed and pressed into pellets using a hydraulic press under a load of 10.4 metric tons. For sample S1, Fe (0.9173 g) and Sb (2 g) of FeSb stoichiometric were used. The pellet was placed in a porcelain crucible and was heated in a furnace at 600°C for 2 hours, followed by 900°C for another 2 hours. Nitrogen gas was introduced to minimize oxygen interaction with the alloy components at high temperatures. The sample was then slowly cooled to room temperature, whereas the gas flow was stopped when the temperature reached 700°C. Afterwards, the FeSb alloy was ground using a mortar and pestle, re-pressed into a pellet, and reheated at 850°C for 7 hours under continuous nitrogen flow. Sample S2 was prepared using the same procedure as S1, but with a doubled nitrogen gas flow rate and a heating step at 850°C for 5 hours. The sample was composed of Fe (0.99942 g) and Sb (1.3 g) of Fe_2Sb stoichiometric. Sample S3 was prepared using Fe (0.56 g) and Sb (1.2192 g) of FeSb stoichiometric. The pellet was placed between two tungsten boats inside a vacuum chamber evacuated to a pressure of 10^{-5} Torr as shown in Fig.1. It was then heated by passing an electric current through the boats. The current was applied in stages as follows: 80 A for 30 minutes, 160 A for 40 minutes, 200 A for 50 minutes, and finally 80 A for 70 minutes. After each stage, the product was ground and re-pressed into a pellet. Finally, the sample was left to cool inside the chamber for over 30 minutes to ensure it reached room temperature and to prevent oxidation.

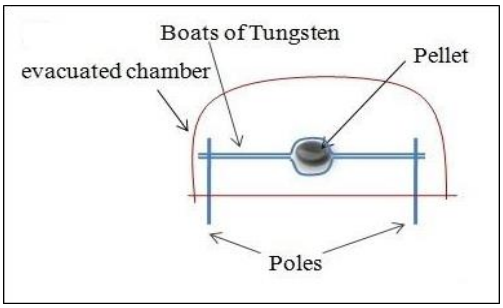

Fig.1. Schematic diagram of the system used for heating the pellet.

3 Results and Discussion

As shown in the EDX spectrum in Fig. 2, the gas flow used in samples S1 and S2 was not sufficient to prevent oxygen incorporation. In contrast, the oxygen content in sample S3 was very low, which is expected, as some residual oxygen may have remained between the powder grains during the pressing process. This suggests that oxygen in S3 formed a phase with antimony, unlike the combustion-like reaction observed in S1 and S2. Therefore, it is preferable to perform the mixing and pressing processes inside a glove box to limit exposure to atmospheric oxygen. Sample S1 exhibited a dark red color, which suggests iron oxidation. On the other hand, sample S2 showed the presence of spherical Sb_2O_3 particles [15,16,17], as observed in the SEM image in Fig. 3. Sample S3, by contrast, appeared dark silver in color.

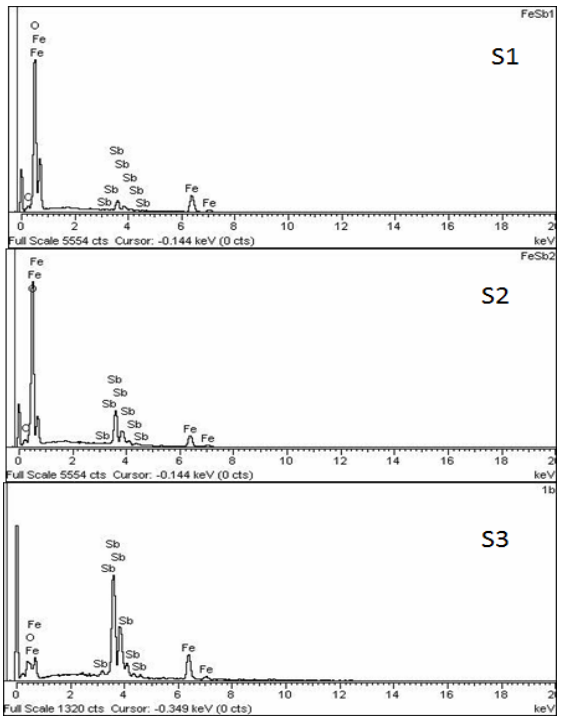

Fig. 2. EDX spectra of S1, S2, and S3 samples.

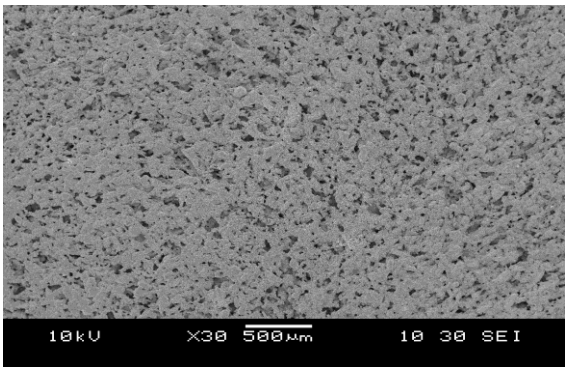

Fig.3. SEM for sample S1 show the spherical Sb_2O_3 particles

SEM was utilized to analyze the surface morphology of samples S1, S2, and S3, as shown in Fig.4. Sample S1's dense, compact microstructure may be due to partial melting or sintering during high-temperature processing with oxygen, resulting in the formation of iron oxides, as supported by the dark red coloration observed visually. In contrast, sample S2's microstructure appears more porous and granular, with fine, loosely packed particles. The SEM image reveals the presence of spherical and irregularly shaped grains, which are consistent with the formation of Sb_2O_3 as a result of oxidation. This finding aligns with the EDX results, which indicated relatively high oxygen content in both S1 and S2. However, the dispersed nature of grains in S2 indicates a less uniform reaction process and potentially higher oxidation rate compared to S1. Sample S3 exhibits a compact, layered morphology with well-defined grain structures, smoother surfaces, and minimal oxidation, indicating improved structural integrity. This improvement is attributed to the different synthesis method used in S3, which involved a vacuum environment and high electrical current heating. These conditions effectively limited oxygen exposure, as confirmed by EDX analysis, and promoted a more controlled phase formation. We expect the dark silver color of sample S3 to indicate the absence of significant oxidation products.

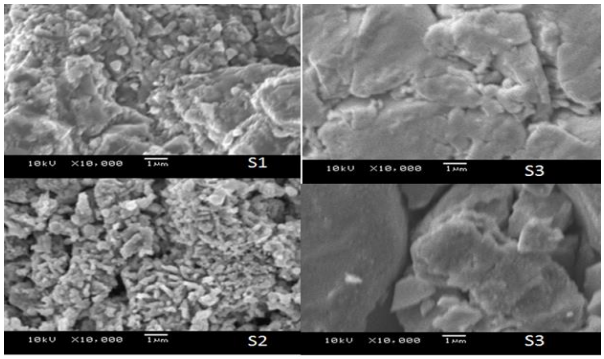

Fig.4. SEM images of the synthesized samples S1, S2, and S3.

The X-ray diffraction analysis of the sample S3, as shown in Fig.5 and table1, indicates the formation of multiple phases. The primary phase identified is $FeSb_2$, confirmed by several strong peaks at 30.62°, 31.32°, 34.75°, and 50.65°. The crystallographic parameters of the $FeSb_2$ phase were orthorhombic, with a=5.830, b=6.550, and c=3.2040 Å, which are in reasonable agreement with previous studies (a=5.815, b=6.517, and c=3.190 Å) [4]. The synthesis conditions led to the formation of iron antimonide with 1:2 stoichiometry, and the presence of secondary phase, elemental antimony (Sb), with dominant peaks at 23.61°, 28.64°, and 41.89°. The presence of Sb implies a slight excess of antimony or incomplete reaction with Fe. A minor amount of metallic iron was detected, most notably by the peak at 44.66°. This suggests that a portion of iron did not participate in compound formation, possibly due to stoichiometric imbalance or kinetic limitations. Furthermore, a very weak peak at 35.34° matches antimony oxide (Sb_2O_3), indicating minimal oxidation. This can be likely due to remaining oxygen trapped during the sample preparation. To minimize such oxidation, it is preferable to perform the mixing and

pressing processes inside a glove box under inert atmosphere. Overall, the XRD pattern confirms that $FeSb_2$ is the dominant phase, accompanied by unreacted Sb, small amounts of Fe, and traces of Sb_2O_3. These results align with expectations for a Fe-rich synthesis under limited oxygen conditions, although further optimization could improve phase purity and reduce secondary components.

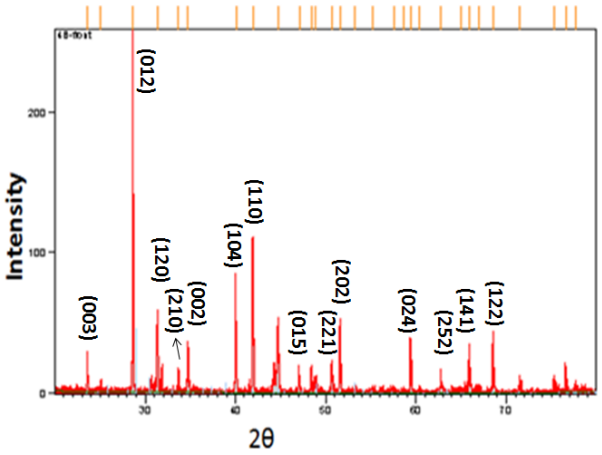

Fig.5. XRD pattern of the synthesized sample (S3).

Table1. List of major diffraction peaks observed in the XRD pattern of the sample S3, along with their corresponding phases.

2θ	Phase
23.61	Sb
25.12	Sb
28.64	Sb
30.62	$FeSb_2$
31.32	$FeSb_2$
33.64	$FeSb_2$
34.75	$FeSb_2$
35.34	Sb_2O_3
40.02	Sb
41.89	Sb
44.25	$FeSb_2$ / Sb_2O_3
44.66	Fe Main
47.04	Sb
48.86	$FeSb_2$ / Sb
50.65	$FeSb_2$
51.55	Sb
59.36	Sb
62.76	$FeSb_2$
65.91	$FeSb_2$
68.55	$FeSb_2$
71.52	$FeSb_2$
75.34	$FeSb_2$
76.56	Sb

4 Conclusion

The study highlights the importance of synthesis conditions, particularly atmospheric control, in determining the structural and compositional quality of Fe-Sb alloy systems. Among the three samples studied, only the sample synthesized under vacuum conditions (S3) exhibited significantly reduced oxidation and a higher degree of phase purity, with $FeSb_2$ emerging as the dominant phase. XRD analysis confirmed the presence of secondary phases such as Sb, Fe, and minor Sb_2O_3 in varying amounts across the samples, consistent with SEM and EDX observations. Notably, the S3 sample was synthesized using a vacuum-assisted thermal process in which the pellet was placed between two tungsten boats and heated via electrical current passed through the boats' terminals. This method not only ensured uniform heat distribution but also minimized exposure to atmospheric oxygen throughout the reaction. The heating configuration was crucial in reducing oxidation and facilitating the controlled formation of intermetallic phases. The findings highlight that vacuum-based current heating, combined with appropriate handling techniques such as glove box pressing, is highly effective in reducing oxygen incorporation and enabling the formation of structurally stable $FeSb_2$ phases. Future work should focus on optimizing the Fe:Sb ratio and refining thermal parameters to further enhance phase purity and suppress residual metallic and oxide components.

References

Bentien, A., Johnsen, S., Madsen, G. K. H., Iversen, B. B., and Steglich, F. (2007). Colossal Seebeck coefficient in strongly correlated semiconductor $FeSb_2$. *EPL (Europhysics Letters)*, *80*(1), 17008. https://doi.org/10.1209/0295-5075/80/17008

Du, Q., Wu, L., Cao, H., Kang, C., Nelson, C., Pascut, G. L., Besara, T., Siegrist, T., Haule, K., Kotliar, G., Zaliznyak, I., Zhu, Y., and Petrovic, C. (2021). Vacancy defect control of colossal thermopower in $FeSb_2$. *Npj Quantum Materials*, *6*(1). https://doi.org/10.1038/s41535-020-00308-z

Saleemi, M., Tafti, M. Y., Jacquot, A., Jägle, M., Johnsson, M., and Toprak, M. S. (2016). Chemical synthesis of iron antimonide ($FeSb_2$) and its thermoelectric properties. *Inorganic Chemistry*, *55*(4), 1831–1836. https://doi.org/10.1021/acs.inorgchem.5b02658

Petrovic, C., Kim, J. W., Bud'ko, S. L., Goldman, A. I., Canfield, P. C., Choe, W., & Miller, G. J. (2003). Anisotropy and large magnetoresistance in the narrow-gap semiconductor $FeSb_2$. *Physical Review. B, Condensed Matter*, *67*(15). https://doi.org/10.1103/physrevb.67.155205

Petrovic, C., Lee, Y., Vogt, T., Lazarov, N., Bud'ko, S., and Canfield, P. (2005). Kondo insulator description of spin state transition in $FeSb_2$. *Physical Review B*, *72*(4). https://doi.org/10.1103/physrevb.72.045103

Cadeville, M. C., and Mirebeau, I. (1983). Magnetic and static lattice perturbation in dilute FeSb alloys from diffuse scattering of unpolarised and polarised neutrons. *Journal of Physics F Metal Physics*, *13*(12), 2449–2463. https://doi.org/10.1088/0305-4608/13/12/006

Zhu, Z., Su, X., Yin, F., Tu, H., and Wu, C. (2009). 450°C isothermal section of the Zn–Fe–Sb ternary phase diagram. *Journal of Alloys and Compounds*, *490*(1–2), 541–547. https://doi.org/10.1016/j.jallcom.2009.10.077

Kumari, L., Li, W., Huang, J. Y., and Provencio, P. P. (2010). Nanosize Transition Metal Antimonides, NISB and $FeSb_2$: Solvothermal synthesis and Characterization. *The Journal of Physical Chemistry C*, *114*(21), 9573–9579. https://doi.org/10.1021/jp9110053

Abbassi, L., Mesguich, D., Coulomb, L., Chevallier, G., Aries, R., Estournès, C., Flahaut, E., Viennois, R., and Beaudhuin, M. (2022). In-situ reactive synthesis of dense nanostructured β-FeSi2 by Spark Plasma Sintering. *Journal of Alloys and Compounds*, *902*, 163683. https://doi.org/10.1016/j.jallcom.2022.163683

Fayez, T. M., Zeyara, W. a. M., Salem, F. M. A., Malek, H. M. A., and Ahmed, M. M. A. (2018). Time dependence of the resistivity of the Fe-Sb system at room temperature. *The International Journal of Physics*, *6*(2), 30–32. https://doi.org/10.12691/ijp-6-2-1

Tomczak, J. M. (2018). Thermoelectricity in correlated narrow-gap semiconductors. *Journal of Physics Condensed Matter*, *30*(18), 183001. https://doi.org/10.1088/1361-648x/aab284

Safaie, N., Khakbiz, M., Sheibani, S., and Bagha, P. S. (2015). Synthesizing of nanostructured Fe-Mn alloys by mechanical alloying process. *Procedia Materials Science*, *11*, 381–385. https://doi.org/10.1016/j.mspro.2015.11.134

Sun, Y., Liu, J., Fan, X., Li, Y., and Peng, W. (2023). Synthesis and application of iron sulfide−based materials to activate persulfates for wastewater remediation: a review. *Frontiers in Environmental Science*, *11*. https://doi.org/10.3389/fenvs.2023.1212355

Duan, Y., and Sun, J. (2023). Preparation of Iron-Based sulfides and their applications in biomedical fields. *Biomimetics*, *8*(2), 177. https://doi.org/10.3390/biomimetics8020177

Qi, W., Guo, S., Sun, H., Liu, Q., Hu, H., Liu, P., Lin, W., & Zhang, M. (2022). Synthesis and characterization of Sb2O3 nanoparticles by liquid phase method under acidic condition. *Journal of Crystal Growth*, *588*, 126642. https://doi.org/10.1016/j.jcrysgro.2022.126642

Validžić, I. L., Abazović, N. D., Mitrić, M., Lalić, M. V., Popović, Z. S., & Vukajlović, F. R. (2012). Novel organo-colloidal synthesis, optical properties, and structural analysis of antimony sesquioxide nanoparticles. *Journal of Nanoparticle Research*, *15*(1). https://doi.org/10.1007/s11051-012-1347-x

Jabeen, S., Veg, E., Bala, S., & Khan, T. (2024). Synthesis, Characterization, and Photocatalytic Activity of Sb2O3 Nanoparticles: A Step towards Environmental Sustainability. *Eng. Proc. 2024, 67(1), 8*, 8. https://doi.org/10.3390/engproc2024067008